Design, Construction and Performance of a Buck-Boost Converter for an Ultracapacitor-Based Auxiliary Energy System for Electric Vehicles

Micah Ortúzar, Juan Dixon (SM IEEE) and Jorge Moreno
Department of Electrical Engineering
Pontificia Universidad Católica de Chile
Casilla 306, Correo 22, Santiago, Chile
Fax: 56-2-552-2563, e-mail: mortuzad@puc.cl

***Abstract*. This paper describes step by step the process of designing, constructing and testing a bidirectional Buck-Boost converter. This converter was conceived to be used as a controlled energy-transfer-equipment between the main energy source of an electric vehicle (a battery pack in this case) and an auxiliary energy system based on Ultracapacitors. The converter is able to transfer energy in both directions, at rates of more than 40kW. The battery pack's nominal voltage is 330V, while the Ultracapacitor's voltage depends on their state of charge (SOC), ranging from 100V to 300V. Equations governing current transfer and current ripple are analyzed. These equations will be used as guidelines for the control system design and smoothing inductor size requirement. The topology used is a Buck-Boost configuration. Special care had to be taken in designing the smoothing inductor and managing thermal loses, for these are critical to the overall performance. The inductor constructed, rating 1.5mH, is capable of transferring 200A for several minutes with low loses and no core saturation (air core was used). A special water-cooled heatsink was designed and constructed, whit a very low volume of less than 900 cc and a thermal resistance of less than 0.011ºC/W. The control system was implemented on a TMS320F241 DSP from Texas Instruments, which consists in two control loops. The first one controls the converter's current, using as a reference the value obtained from the second loop, which controls the Ultracapacitors State Of Charge (SOC). Criteria ruling this second loop are not discussed in this paper. Finally, some experimental results of the overall system are displayed.**

I. INTRODUCTION

Electric vehicles have improved their performance and made suitable for commercial and domestic use during the last decades. Nevertheless, pure electric vehicles still have not achieved ranges comparable to that of gas powered conventional vehicles. This problem, due to the low energy density and specific energy contained in most electric batteries compared to that of gasoline, is resolved in hybrid vehicles by combining high energy density of gas or hydrogen and high efficiency of electric drive systems [1].

Still, gas-based or hydrogen-based energy storage systems, unlike batteries, are unable to accept energy from regenerative braking. For this reason, hybrid systems use an auxiliary energy system that is able to receive regeneration from the drive train and that serves as a power cache for peak power phenomena. This allows using energy systems (gas turbines, fuel cells, etc) with lower power ratings, similar to the mean power consumption, and at the same time increase the overall vehicle efficiency [2]. Two topologies can be distinguished regarding auxiliary energy system connection, parallel and serial connections. Fig. 1 shows a serial connection of a generic hybrid vehicle, often used in vehicles running on fuel cells or Zinc-Air batteries.

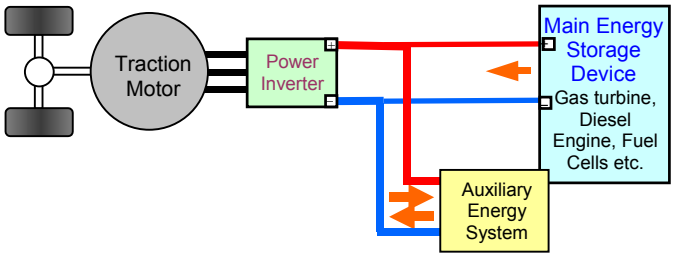

Fig. 1. Power circuit of a typical serial hybrid vehicle.

Series Hybrid Vehicles are those in which all energy coming from the energy source goes thorough the electric traction motor.

Parallel Hybrid Vehicles are those in which mechanic energy is delivered to the main traction shaft from an electric motor and an internal combustion motor, using a special gearbox (usually a planetary gearbox).

Considering a typical city drive cycle, the auxiliary energy system should have regeneration capability, medium-low energy content (enough for enduring short acceleration periods and accepting regenerative braking), a high power capability (in order to complement the mean-power-sized energy storage device to satisfy peak power demand) and low-losses characteristic [2]. These requirements lead to such storage devices as high-power batteries, flywheels and Ultracapacitors as the most adequate for auxiliary energy systems.

Parallel-connected hybrid topology, shown in Fig. 1, may also be applied to battery-powered vehicles [3]. In cases in which battery performance at high power is poor due to high loses and implies life shortening, or when using batteries that do not accept regeneration, as in Zinc-Air batteries, the addition of an auxiliary energy system as the one described may help reducing loses and increasing available power, while extending the battery's life.

An auxiliary energy system, based on Ultracapacitors and a bidirectional Buck-Boost converter was designed and constructed with the purpose of installing it on an existing electric vehicle. The electric vehicle was transformed at the Universidad Católica de Chile from a conventional Chevrolet LUV truck, similar in shape and size to a Chevrolet S-10

0-7803-7906-3/03/$17.00 ©2003 IEEE.

light pick-up truck [4]. The vehicle uses a brushless dc motor with a nominal power of 32 kW, and a peak power of 53 kW. The main energy storage system consists of 26 lead-acid batteries connected in series. These batteries have a high internal resistance; producing considerable loses at high power demand and also shortening batteries life whenever hydrogen evaporation is produced (when any battery's voltage surpasses 13.8V). The auxiliary energy system is intended to prevent batteries from delivering or accepting high currents by sensing the load current and delivering or accepting the difference. Batteries are also not capable of properly accepting regenerative braking energy when recently charged, generally resulting in battery damage; this would also be fixed with the auxiliary system by preventing batteries from overcharging.

Fig. 2 shows the vehicle's power circuit schematic with parallel auxiliary system. The DC-DC Buck-Boost converter's design and construction process is described in this paper.

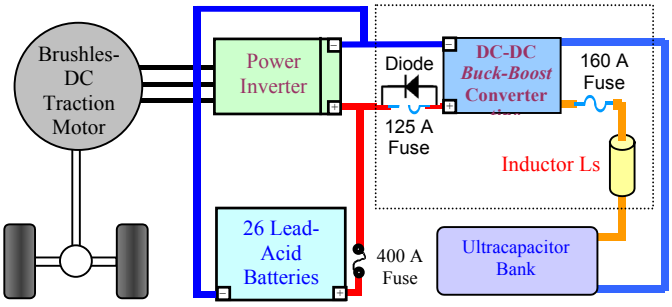

Fig. 2. Resulting power circuit in electric vehicle.

II. BUCK-BOOST TOPOLOGY ANALYSIS

Because the Ultracapacitor-bank's estimated resulting capacitance of 20.45F (132 2700F capacitors in series) is considered large enough, the Ultracapacitor bank will be modeled as a constant voltage source for periods of time up to several seconds.

Fig. 3 shows a simplified schematic of the Buck-Boost converter and the two connected sources. The Ultracapacitor bank is considered as a constant voltage source (*V2*) with a series resistance and the battery pack (*Vdc*) as an ideal voltage source with its internal series resistance.

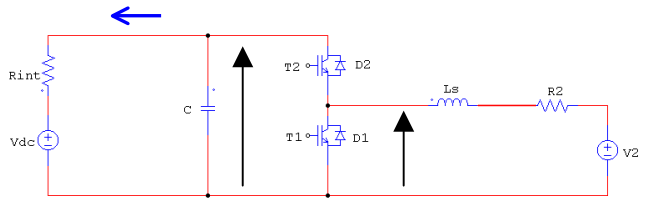

Fig. 3. Buck Boost converter schematic.

The converter itself is composed of the inductor *Ls*, the capacitor *C,* IGBTs *T1* and *T2*; and Diodes *D1* and *D2*. A 12kHz fixed-frequency PWM is applied on either IGBT to transfer energy back and forth. Buck operation consists of transferring energy from the Battery pack to the Ultracapacitors by triggering IGBT *T2*. Boost operation results from triggering IGBT *T1*, in this way energy is transferred from the Ultracapacitor to the Battery pack. However, on either case the amount of current transferred, if any at all, will depend on the Ultracapacitor's actual voltage, the system parameters (resistances values, battery voltage) and the duty cycle of the PWM applied. While the energy-transfer's efficiency will depend on these conditions and on the semiconductor's loses. Equations governing the converter will be discussed further on.

In the steady state and for mean values during periods of several seconds, the converter can be modelled as an ideal DC transformer as follows.

For the Boost operation, steady state voltages and currents are described by equations (1) and (2), respectively [5]. For simplicity, these equations do not take into account the diode's and IGBT's voltage drop effect.

$$\overline{Vc} = \frac{Vs}{(1-\delta)} \tag{1}$$

$$\overline{Ib} \approx \begin{cases} \dfrac{\left(V2/(1-\delta) - Vdc\right)}{\left(R\,\mathrm{int} + R2/(1-\delta)^2\right)} & V2/(1-\delta) - Vdc \geq 0 \\ 0 & V2/(1-\delta) - Vdc < 0 \end{cases} \tag{2}$$

In equations (1) and (2) *V2* stands for the Ultracapacitor voltage, *Vdc* for the Battery voltage, *Rint* for the Battery's internal resistance, *R2* for the sum of the inductor's resistance and the Ultracapacitor's ESR (Equivalent Series Resistance); and δ stands for the duty cycle of the PWM applied. As it can be seen in eqs (1) and (2), Boost operation can be modelled as a one-way-conducting DC transformer, where the transformer ratio seen from the Ultracapacitor side is $1/(1-\delta)$.

Equations (3) and (4) describe steady state voltages and currents during Buck operation.

$$\overline{Vs} = \delta \cdot Vc \tag{3}$$

$$\overline{Ib} \approx \begin{cases} -\dfrac{(Vdc \cdot \delta - V2)}{(R2 + R\,\mathrm{int} \cdot \delta^2)} & (Vdc \cdot \delta - V2) \geq 0 \\ 0 & (Vdc \cdot \delta - V2) < 0 \end{cases} \tag{4}$$

As in the previous case, Buck operation may be modelled as a one-way-conducting DC transformer, where the transformer ratio seen from the battery side is δ.

Equations (2) and (4) do not take into account the ripple component of currents. Equations (1) thru (4) will help understand the converter's behaviour under different conditions and will help elaborate an adequate control strategy.

III. CURRENT RIPPLE ANALYSIS

In order to produce a controlled DC current thorough the Ultracapacitors, small ripple content is desirable. High ripple amplitude also produces other undesired effects, such as loses due to currents induced in other elements; and electromagnetic noise. Therefore, it is desirable to reduce ripple amplitude as much as possible.

Fig. 4 shows a typical steady state current waveform for a Buck operation.

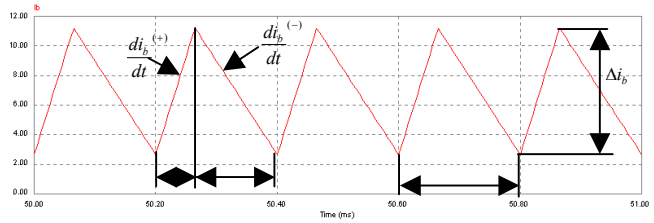

Fig. 4. Current thorough Ultracapacitors ripple waveform.

Equations (5), (6) and (7) describe the relation between current's components signalled in fig. 4, which corresponds to current thorough Ultracapacitors during a Buck operation.

$$\frac{di_b}{dt}^{(+)} = \frac{Vdc - V2}{Ls} = \frac{\Delta i_b}{t0} \qquad (R2 \approx 0, R\,\text{int} \approx 0) \qquad (5)$$

$$\frac{di_b}{dt}^{(-)} = -\frac{V2}{Ls} = -\frac{\Delta i_b}{T - t0} \qquad (R2 \approx 0) \qquad (6)$$

$$\Delta i_b = \frac{Vdc}{Ls \cdot f} \cdot \delta \cdot (1 - \delta) \qquad \left(f = \frac{1}{T}\right) \qquad (7)$$

For simplicity, these equations do not take into account the effect of diode and IGBT voltage drop, nor the voltage drop thorough *R2* and *Rint* resistances.

Deriving with respect to δ and zeroing eq (7) leads to the value of δ for which the ripple amplitude (represented by Δi_b) is maximum. This value is 0.5. Then the maximum value of Δi_b is described by eq (8).

$$\Delta i_b \max = \frac{Vdc}{4 \cdot f \cdot Ls} \qquad (8)$$

As it was mentioned before, the Battery pack's nominal voltage (Vdc) is 330V. The frequency (f) value of 12 kHz was arbitrarily chosen in order to minimize current ripple, while maintaining low commutation loses and operating the IGBT within its recommended range.

A ripple of 5A was established as the maximum desired value. Therefore, the inductance *Ls* value must be of at least 1.38mH.

IV. POWER CIRCUIT DESIGN

For the inductor *Ls* design, several requirements had to be taken into account. First of all, the inductance value had to be of, at least, 1.38mH; its weigh and volume had to be the smallest possible; also, its series resistance had to be minimized.

In order to minimize the skin effect at high frequencies, while maintaining a small volume, a laminated conductor was considered the best choice. Because of its conductivity to weigh ratio (better than copper), aluminum conductor would be used.

Equations (9) thru (11) show relations between the inductance value, core reluctance, magnetic flux density and the inductance's parameters [6].

$$L = \frac{N^2}{R} \qquad (9)$$

$$R = \frac{l}{\mu_r \mu_0 \cdot A} \qquad (10)$$

$$B = \frac{N \cdot I}{R \cdot A} \qquad (11)$$

Where L is the inductance in H, N the number of turns, R the core reluctance, l the core length in meters, A the core section in square meters, μ_0 the air's magnetic permeability, μ_r the core's relative magnetic permeability, B the magnetic flux density in Tesla and I is the current thorough the inductor in Amps. These equations are valid for a cylindrical core inductance.

In order to reach the desired inductance value, a compromise between the number of turns and the resulting core reluctance is established according to eq (9); while both free parameters in this equation, *N* and *R,* have relation with the inductance's volume and weight. On the other hand, both free parameters, *N* and *R*, have influence over the actual magnetic flux density, which must be maintained under the core's saturation flux density over all operating current range (-200A to 200 A). If all these facts are carefully analyzed, one realizes that this is a non-linear-multivariable optimization problem. The formal solution to the problem will not be discussed here, but a general description of the process will be made.

Using air core eliminates the maximum magnetic flux restriction (air does not saturate); therefore equation (11) can be neglected. This liberates variables *l* and *A*, although variable *l* is still restricted by the conductor width (which was established as 12 cm to reduce series resistance). Observing eq (9) it is easy to realize that the number of turns has a quadratic relation with the inductance value, while the reluctance has only an inverse linear relation with it; and therefore, up to some extent, it is more effective to increase the number of turns than it is to increase the core section.

Finally, a two-winding, cylindrical-air-core inductance was designed. Each winding has 133 turns (266 in total); the core has a diameter of 7cm and is 26cm long. The resultant inductance is slightly higher than 1.5mH and, because of its air core, it does not saturate at any current value. The higher inductance value accomplished is probably due to the higher real core diameter produced by packing elements such as insulation paper.

A 0.5mm thick, 12cm wide laminated aluminum conductor was used for the inductor, with a resulting total resistance of 37 mOhm. The inductance is capable of transferring currents up to 200A for several seconds without considerable heating.

The resulting inductance weighted 22kg, which is adequate considering the currents it must withstand.

The Ultracapacitor bank was constructed using 132 capacitors from Epcos connected in series. Each capacitor has a 2700F capacitance, 400A nominal current rating, 2.3V nominal voltage rating and 1mOhm ESR. The bank's resulting capacitance is of 20.45F and it's nominal voltage is of 303.6V. A total energy of 255 Wh can be stored in the Ultracapacitor bank, which is enough to have more than 40kW during 20 seconds.

The IGBT used is an Intellimod, model PM400DSA060 from Powerex. It's collector maximum current is of 400A, the Collector-Emitter maximum voltage is of 600V.

V. THERMAL MANAGMENT

Power loses in the IGBT and diode, due to internal resistance and characteristic voltage drop, presents a semiconductor-destruction hazard if not evacuated properly. To evaluate this hazard, power loses must be estimated and a thermal model elaborated.

Fig. 5 shows a thermal model for an IGBT-diode pair. Restraints are set by the manufacturer for the case temperature (T_c<100ºC), the IGBT juncture temperature (T_{jQ}<110ºC) and the diode juncture temperature (T_{jF}<110ºC) [7].

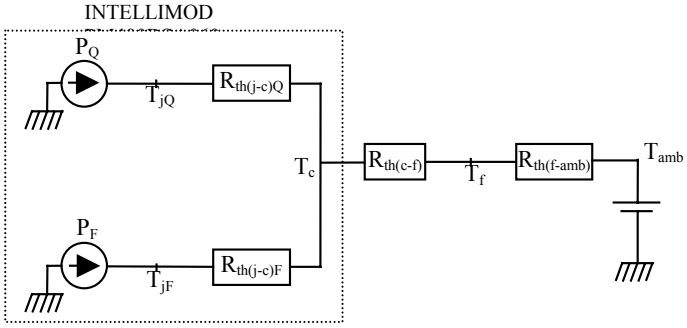

Fig. 5. Thermal model for the semiconductor.

Equations (12), (13) and (14) show the relation between each temperature, power loses and thermal resistances ($R_{th(jc)Q}$, $R_{th(j-c)F}$ and $R_{th(c-f)}$ are specified by the manufacturer).

$$T_c = Tamb + \left(R_{th(c-f)} + R_{th(f-amb)}\right)\cdot\left(P_Q + P_F\right) \quad (12)$$

$$T_{jQ} = Tamb + \left(R_{th(c-f)} + R_{th(f-amb)}\right)\cdot\left(P_Q + P_F\right) + R_{th(j-c)Q}\cdot P_Q \quad (13)$$

$$T_{jF} = Tamb + \left(R_{th(c-f)} + R_{th(f-amb)}\right)\cdot\left(P_Q + P_F\right) + R_{th(j-c)F}\cdot P_F \quad (14)$$

Most probable total power loses where estimated in 240W, where 187.2W corresponds to IGBT loses and 52.8W to diode loses. These estimates where calculated from the weighted sum of conduction and commutation loses over different conditions.

In order to preserve temperatures from rising over the recommended limits while operating under the aforementioned conditions, it was calculated that the heatsink's thermal resistance must be smaller than 0.05ºC/W.

As such a heatsink with specific dimensions could not be found in the market; a water cooled aluminum heatsink was designed and constructed.

Fig. 6 shows the heatsink's scheme with pipes attached. The heatsink consists of two machined aluminum blocks, one formed by one of the faces and the perimeter as a tub; and the other consisting of the other face and the attached cooling fins. These two pieces assembled together form a symmetrical fluid circuit, thorough which water will flow coming from an existing cooling system.

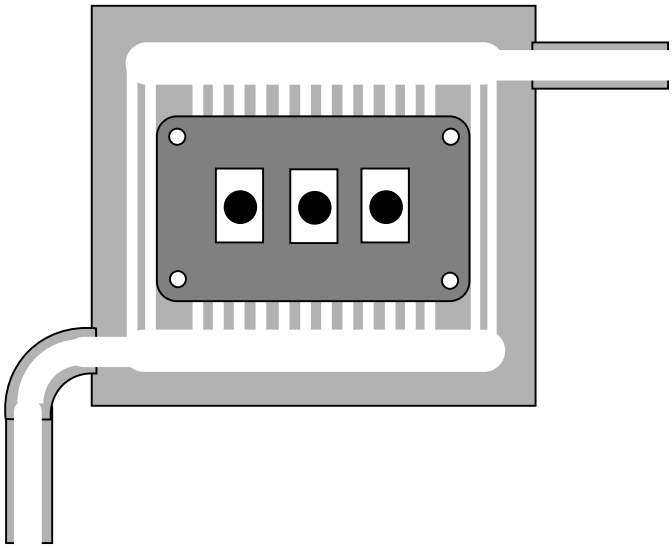

Fig. 6. Aluminum heatsink scheme and Intellimod outline.

Theoretical calculations of the heatsink's thermal resistance where made (using convection equations for plain surfaces and fins attached to plain surfaces [8]). Assuming water flow rate of 5.5 gpm, a thermal resistance of 0.01023ºC/W was calculated. This value satisfies the 0.05ºC/W requirement.

VI. CONTROL SYSTEM

The Control system, conformed by two closed loops, was implemented on a TMS320F241 DSP from Texas Instruments.

Figure 7 shows a schematic flowchart of the control system. Interface transducers and circuitry had to be installed for the DSP to properly acquire data and deliver commanding signals.

Other signals not shown in fig 7, such as the drive train current, are obtained and used in the control algorithm. This algorithm will be superficially described.

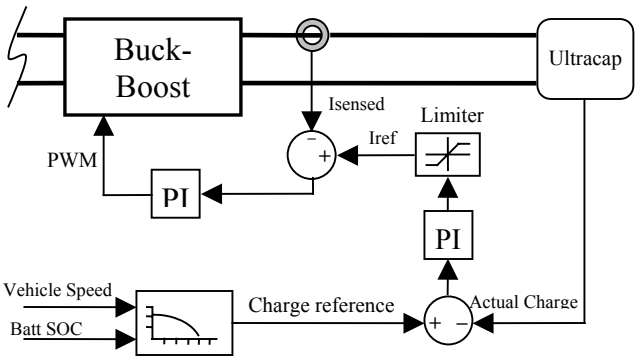

Fig. 7. Control system schematic.

The first loop controls the current thorough the Ultracapacitors. A signal proportional to the Ultracapacitor's current is acquired by the DSP, this value is compared with a pre-established reference and a PI gain is applied to the error obtained. The outcome is traduced into a PWM and delivered to the Buck-Boost converter.

The second loop controls the Ultracapacitor's SOC. The Ultracapacitor's voltage is measured, converted into its SOC equivalent and compared with the SOC reference; a PI gain is applied to the error obtained and, after applying a limiter, the result is delivered to the first control loop as the current reference.

Although the control algorithm is a little more complicated than what is explained here, the main functions are the ones previously exposed.

VII EXPERIMENTAL RESULTS

As expected, the maximum ripple content was produced at duty cycle of 0.5 and its value was of less than 5A (about 4.5A). Figure 8 shows ripple waveforms for buck and boost operations.

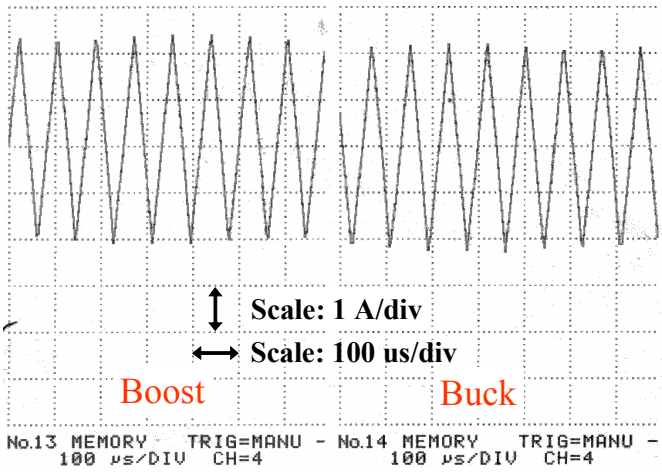

Fig. 8. Maximum current ripple for buck and Boost operation.

A current reference-step-response test was performed on the Buck-Boost converter to see how fast the current control response is. Figure 9 shows two step response curves for maximum current rating, one for buck operation and the other for boost operation.

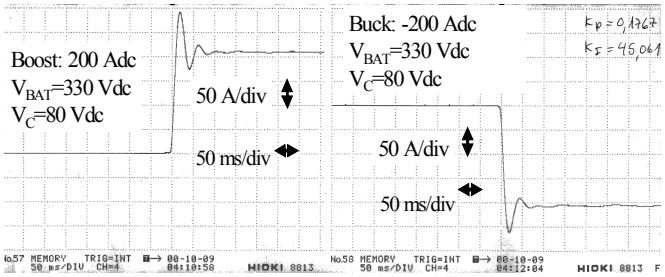

Fig. 9. Current control Step response.

Curves in fig. 9 show that the system has a time constant of less than 100mS. This time constant is short enough for the system to react to reference changes of two hundred amps in one tenth of a second. The main component influencing the time constant is the inductance Ls, because it opposes to current changes introducing a delay in the system response. The control's acquisition time is not considered a gravitating factor in the system's time constant, because the control algorithm is executed 12.000 times per second (as fast as the PWM) the largest delay that could be introduced at the control level would be 1/12.000 S, that is less than 9*10^-5 (less than 1% of the time constant).

Road tests where performed with the auxiliary energy system installed and working. The control algorithm limited battery currents to -3A and 35A, while the balance demanded by the drive train was delivered/absorbed by the auxiliary system.

Figure 10 shows a plot of drive train currents (I Load), Battery currents (I Batt) and Buck-Boost currents (I BB) during a short period of time.

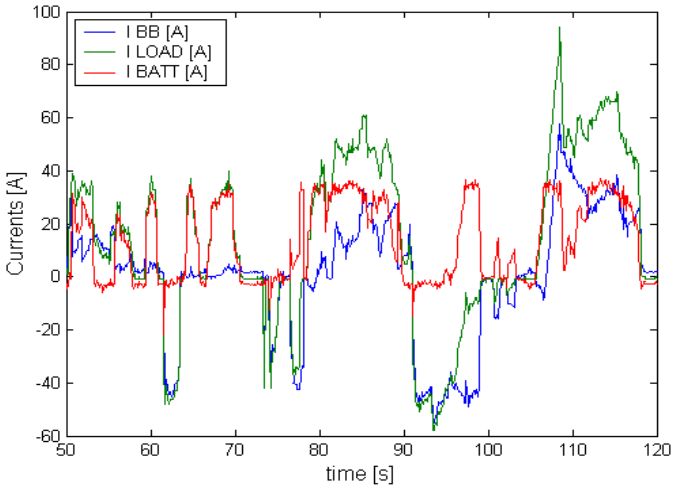

Fig. 10. Road test currents plot

The previous figure illustrates how the battery currents can be limited by means of delivering/absorving the balance of the currents demanded, while the Ultracapacitor's SOC is controlled by setting preferred current levels thorough it when the battery currents are not at its limit.

Finally, it can be said that the system behaved perfectly and that preliminary results show an increase of overall vehicle efficiency of 15%, due to the auxiliary energy system operation. However, these result where achieved in highly congested traffic conditions and cannot be considered as a permanent all-condition result. A thorough test program is being implemented to determine the real increase in efficiency under different conditions.

VIII. CONCLUSIONS

An auxiliary energy system based on Ultracapacitors and a Buck-Boost converter was designed and constructed. The system was installed in an electric vehicle to support the batteries during peak power demand. The converter is capable of transferring up to 200A in either direction at 330V.

A specially designed smoothing inductor was constructed. The inductor, rating 1.5mH, is capable of conducting 200A during several seconds without considerable heating, due to low series resistance. Air core was used to prevent saturation.

A water-cooled heatsink of less than 0.011ºC/W was designed and constructed. The thermal resistance achieved is low enough for the converter to work properly along its power range without overheating danger.

Ultracapacitor currents showed a maximum ripple of less than 5A, as expected. Current step-reference-change test showed an adequate time constant of less than 0.1S,which is considered low enough for the slow-changing current references.

Road tests with the auxiliary system installed showed excellent results regarding system behavior and efficiency increase as well. Overall vehicle efficiency increase due to the auxiliary energy system was estimated at about 15%, which is considered an excellent preliminary result.

IX. ACKOWLEDGEMENTS

The authors want to thank Conicyt through *Project Fondecyt 1020982,* for the support given to this work.

X. REFERENCES

[1] Osamu Fuji, "The Development and Application of Hybrid Vehicles". *19th Electric Vehicle Symposium*, Busan, korea, October, 2002.

[2] Per Rutquist, "Optimal Control for the Energy Storage in a Hybrid Electric Vehicle" *19th Electric Vehicle Symposium*, Busan, korea, October, 2002.

[3] Jin-uk Jeong, Hyeoun-dong Lee, Chul-soo Kim, Hang-Seok Choi and Bo-Hyung Cho, "A Development of an Energy Storage System for Hybrid Electric Vehicles Using Supercapacitor". *19th Electric Vehicle Symposium*, Busan, Korea, October, 2002.

[4] J. Dixon, M. Ortúzar, R. Schmidt, G. Lazo, I. Leal, F. García, M. Rodríguez, A. Amaro and E. Wiechmann, "Performance Characteristics of the First, State-of-the-art Electric Vehicle Implemented in Chile", *17th Electric Vehicle Symposium*, Montreal, Canada, October, 2000

[5] M.Rashid, "Pulsadores en CD", *Electrónica de Potencia; Circuitos, Dispositivos y Aplicaciones*, Capítulo 9. 2nd Edition, Pearson Education.

[6] D. Halliday and R. Resnick, Física, Capítulo 36 "La Inductancia". 8ª edición Compañía Editorial Continental.1988.

[7] Powerex, Inc. "*IGBTMOD and Intellimodtm – Intelligent Power Modules, Applications and Technical Data Book"*. First edition. Published by Powerex, Inc. 1994.

[8] A. Chapman, *Heat Tansfer*, Third Edition. Macmillan Publishing Co. Inc., 1974, pp 72-76, 334-336.

[9] J.Lott and H. Späth, "Double Layer Capacitors as additional Power Source in Electric Vehicles". *18th Electric Vehicle Symposium*, Berlin, Germany, Octubre, 2001.